MODULATION DOMAIN REFERENCE POINT DETECTION FOR FINGERPRINT RECOGNITION

Nantapol Kitiyanan and Joseph P. Havlicek

School of Electrical and Computer Engineering
University of Oklahoma, Norman, OK 73069
E-mail: yongie@ou.edu joebob@ou.edu

ABSTRACT

Accurate fingerprint reference point detection is one of the most important steps in automatic fingerprint identification process. The fingerprint reference point is defined as the location where the maximum in concave ridge curvature is detected. In this paper, we present a multi-resolution reference point detection algorithm based on Poincaré index in the computed AM-FM modulation domain. Performance of the proposed algorithm is analyzed by comparing with the multi-resolution approach based on integration of sine components in two adjacent regions [6]. The experimental results from applying the proposed method over the FVC 2000 Database 2 [11] show that our algorithm outperformed the competing algorithm in term of detection accuracy and consistency.

1. INTRODUCTION

Automatic fingerprint recognition has been increasingly used in several identification and verification applications such as access controls for security locations or personal belongings. The ideal fingerprint recognition algorithm should tolerate translation, orientation, elastic distortion, and noise from the input fingerprints. In order to match two fingerprints which are usually interfered by those unknown distortions and noises, the fingerprints must be registered with respect to each other or to some well-defined reference points. In [6], the north most loop type singularity (core), the point where the curvature in concave ridges is maximum, was chosen to be the reference point.

Since fingerprint images can be considered as oriented texture patterns and have well defined local frequencies and orientations, AM-FM *Dominant Component Analysis* (DCA) [1-4] can be properly used in order to represent such texture images. By using the same reference point definition as declared in [6], we present a new multi-resolution algorithm that uses Poincaré index in computed AM-FM modulation domain for performing reference point detection.

This paper is organized as follows. A brief review of AM-FM DCA is given in section 2. In section 3, we present a new pixel-based fingerprint segmentation algorithm based on the designed filterbank and channel selection criterion. In section 4, we represent local ridge orientation field of fingerprint images using vector-valued dominant FM functions. The reference point algorithm is presented in section 5 followed by the experimental results in section 6 and conclusion in section 7.

2. AM-FM IMAGE MODELS

AM-FM functions are nonstationary quasi-sinusoidal oscillations that admit simultaneous amplitude and frequency modulations [2]. Let *s(x,y)* be a real valued fingerprint image. Let *t(x,y)* be the complex *analytic image* associated with *s(x,y)* from adding a 2-D directional Hilbert transform of the image itself as its imaginary part [5]. 2-D multi-component AM-FM fingerprint image then takes the form [1-4]

$$t(x,y) = \sum_{k=1}^{K} t_k(x,y) = \sum_{k=1}^{K} a_k(x,y)\exp[j\varphi_k(x,y)]. \quad (1)$$

$a_k(x,y) \geq 0$ is the *amplitude modulation function*, or *AM function* of component $t_k(x,y)$ and $\nabla\varphi_k(x,y)$ is the *frequency modulation function* or *FM function* of component $t_k(x,y)$. The AM function $a_k(x,y)$ captures the local contrast of the complex-valued image $t_k(x,y)$, while the FM function $\nabla\varphi_k(x,y)$ captures the local texture orientation and granularity. The vector-valued FM function may be further decomposed into an instantaneous horizontal frequency function $U_k(x,y) = [1\ 0]\nabla\varphi_k(x,y)$ and instantaneous vertical frequency function $V_k(x,y) = [0\ 1]\ \nabla\varphi_k(x,y)$.

One well-known method for isolating the multiple image components in (1) from each other is to apply a multi-band Gabor filterbank as described in [4]. Estimations of each component AM-FM function, $a_k(x,y)$ and $\nabla\varphi_k(x,y)$, can be perform from the complex channel responses of the filterbank. Let $y_i(x,y)$ be the channel response of the Gabor filter G_i dominated by image component $t_k(x,y)$ at a particular point (x,y). The estimate of AM and FM functions of component $t_k(x,y)$ at the point (x,y) can be obtain using the local nonlinear algorithm [2]

$$\nabla\varphi_k(x,y) \approx \mathrm{Re}\left[\frac{\nabla y_i(x,y)}{j y_i(x,y)}\right], \quad (2)$$

and $$a_k(x,y) \approx \left| \frac{y_i(x,y)}{G_i[\nabla \varphi_k(x,y)]} \right|. \quad (3)$$

It is possible to extract the dominant modulations on a pointwise basis. This approach is known as *Dominant Component Analysis,* or DCA [1-4]. At each pixel, the dominant modulations are the AM and FM functions that correspond to the component in (1) that dominates the local image spectrum. The dominant component, that locally dominate image spectrum, is defined as the one that dominates the response of the channel that maximizes a channel selection criterion [2-4]

$$\Psi_i(x,y) = \frac{\left| y_i(x,y) \right|}{\max_{\omega_1,\omega_2} \left| G_i(\omega_1,\omega_{2)} \right|}. \quad (4)$$

The DCA provides a powerful characterization of the local texture structure and has been used with great success in solutions to a wide variety of image processing and computer vision problems [1-4].

3. FILTERBANK DESIGN AND SEGMENTATION

As stated in the previous section, a bank of Gabor filters is usually used for isolating image components in (1) from each other. Since fingerprint images have well defined local structures, frequencies, and orientations, instead of utilizing a filterbank that covers every point in the right half of the spatial frequency plane as described in [4], a properly tuned Gabor filterbank can be employed to capture such structures. This will greatly reduce the processing time required in the DCA process. As a result, we use a bank of sixteen Gabor filters to isolate image components, capture ridge structures, and remove unwanted areas.

The first eight Gabor filters are designed to capture ridges and valleys of the fingerprint. Their radial center frequencies are tuned to the average ridge frequency of the fingerprint. The average ridge frequency is defined as the inverse of the average inter-ridge distance. The other eight Gabor filters are mainly designed to remove the background areas which mostly locate at lower radial frequencies. Thus, let the average ridge frequency be *f* cycle per image. We assigned the filterbank design parameter values to: $r_0 = f /$ R cycle per image, R = 1.8, B = 1.0 octave, and η = 0.5. The meaning of these parameters was explained in great details in [4]. With the limitation of two filters per ray, the filterbank arranges in a polar wavelet-like tessellation along the eight rays with two filters per ray. Figure 1(a) shows an example of the filterbank in the frequency domain applicable to 256x256 fingerprint images with average ridge frequency 0.1 cycles per pixel. Figure 1(b) exhibits the filter index assigned to each filter. The filter index will be useful in the segmentation process.

Our segmentation algorithm is the pointwise segmentation based on the exploitation of the designed Gabor filterbank and the channel selection criterion (4). Note that *i* in (4) in our design is ranging from 0 to 15. Let *s(x,y)* be a given fingerprint image. The algorithm begins by constructing an image *m(x,y)* such that each pixel *m(x,y)* contains the index of the filter that maximizes the channel selection criterion at the corresponding pixel *s(x,y)*. The pixel *s(x,y)* is determined to be the foreground pixel if the corresponding pixel *m(x,y)* is equal to 1, 3, 5, 7, 9, 11, 13, or 15. Otherwise, the pixel *s(x,y)* is assigned to be in the background area.

In general, the algorithm leads to a noisy segmentation where spurious small areas of the foreground show up inside a larger area of the background and vice versa. In order to acquire more meaningful segmentation, post-processing is required. Figure 3(b) shows an example of the proposed segmentation algorithm without postprocessing.

There are many different post-processing methods, *e.g.* region growing, active contour model, and morphology, that could be applied to remove the unwanted spurious areas. We have chosen to apply morphological binary open-close filter to smooth the boundary of the segmented cluster. Consequently, we applied a connected component labeling and binary minor region removal to eliminate excess spurious regions. These basic methods can be found in many standard digital image processing textbooks such as [3, 7]. Figure 2 shows an example result from applying the algorithm to a fingerprint image.

4. ORIENTATION FIELD ESTIMATION

In this section, we present the algorithm that estimates fingerprint local orientation field from the vector-valued dominant FM functions. The algorithm was adopted from the algorithm proposed in [8, 9].

Let $U_D(x,y) = \partial \varphi_D(x,y) / \partial x$ be the *dominant horizontal frequency* and $V_D(x,y) = \partial \varphi_D(x,y) / \partial y$ be the *dominant vertical frequency* of $\nabla \varphi_D(x,y)$. Consider representing the vector in the complex plane formed by combining $U_D(x,y)$ and $V_D(x,y)$ as $U_D(x,y) + iV_D(x,y)$, where $i^2 = -1$. To double the angles, we square the vector $U_D(x,y)+iV_D(x,y)$.

Let $U_{s,D}(x,y) = U_D^2(x,y) - V_D^2(x,y)$ and $V_{s,D}(x,y) = 2U_D(x,y)V_D(x,y)$ be the horizontal and vertical of the squared vectors respectively. Let $\theta(i,j)$ be the estimate dominant frequency orientation for a *w x w* window centered at (x_i,y_j). Averaging the double angles in a local *w x w* window is simply performed by separately averaging the two components ($U_{s,D}(x,y)$ and $V_{s,D}(x,y)$):

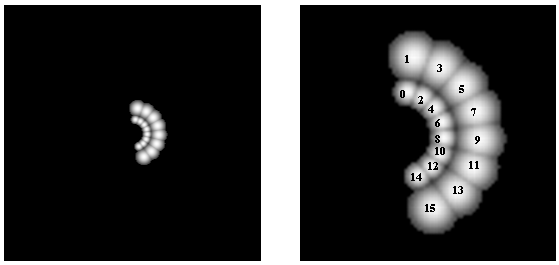

(a) (b)

Figure 1: (a) Frequency domain representation of multiband Gabor filterbank designed to capture ridges of a fingerprint image and for isolating fingerprint image components from one another on a spatio-spectrally localized basis. The filterbank composes of 16 Gabor filters arranged in a polar wavelet-like tessellation along eight rays with two filters per ray. (b) Display the index number assigned to each filter. Note that each filter has been independently scaled for maximum dynamic range in the available gray levels.

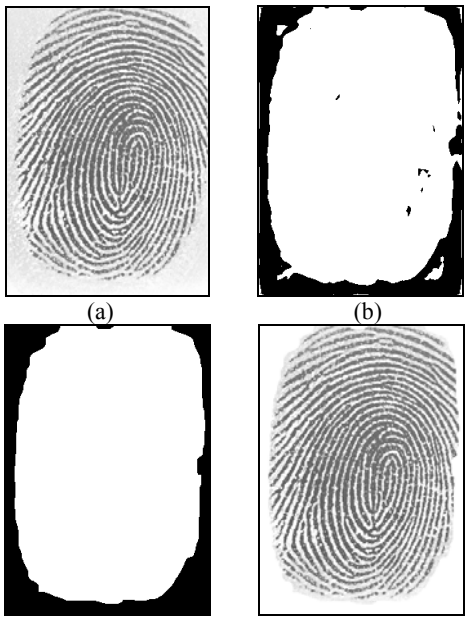

(a) (b)

(c) (d)

Figure 2: An example result from applying the proposed segmentation method to a fingerprint image from FVC2000 Database 2. (a) Input fingerprint. (b) Segmentation without postprocessing. (c) Segmentation result after apply morphological binary open-close filter, connected component labeling, and binary minor region removal. (d) Display the given fingerprint image fused with image (c).

$$J_x(i,j) = \sum_{m=-w/2}^{w/2} \sum_{n=-w/2}^{w/2} U_{s,D}(x_i + m, y_i + n) \quad (5)$$

$$J_y(i,j) = \sum_{m=-w/2}^{w/2} \sum_{n=-w/2}^{w/2} V_{s,D}(x_i + m, y_i + n). \quad (6)$$

Next, the $J_x(i,j)$ and $J_y(i,j)$ are separately smoothed by a mean filter. Let $J_x^{'}(i,j)$ and $J_y^{'}(i,j)$ be the smoothed version of $J_x(i,j)$ and $J_y(i,j)$ respectively. Thus, the estimated local frequency orientation field will be:

$$\theta(i,j) = \frac{1}{2}\tan^{-1}\left(\frac{J_y^{'}(i,j)}{J_x^{'}(i,j)}\right). \quad (7)$$

An example result from applying the algorithm to the fingerprint image in Fig. 2(a) is shown in Fig. 3. The estimated local frequency orientation field is orthogonal to the local ridge orientation field. The equivalent local ridge orientation field $\theta_r(i,j)$, then, can be derived from the local frequency orientation field by:

$$\theta_r(i,j) = \theta(i,j) + \frac{\pi}{2} \quad (8)$$

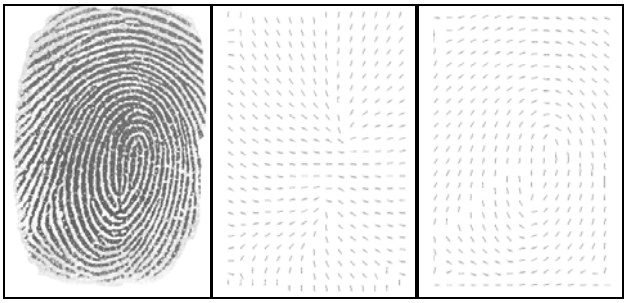

(a) (b) (c)

Figure 3: An example of the AM-FM orientation field estimation applied to fingerprint image (a). (b) Estimated frequency orientation field. (c) Estimated ridge orientation field calculated from the dominant frequency vector field.

5. REFERENCE POINT DETECTION

The proposed reference point detection algorithm in this section is based on the multi-resolution technique. Once the given fingerprint image is segmented, the algorithm is applied on the foreground portion of the image. Started from the coarsest level to the finest level (w = *16, 8, 4*), the algorithm can be summarized as follows:

1. Estimate the AM-FM local frequency orientation field $\theta(i,j)$ using window size of $w \times w$ as described in section 4.
2. Compute the Poincaré index [10, 6] at every block pixel $\theta(i,j)$ in a 2x2 rectangle. The rectangle is traversed in the counterclock wise direction started from the upperleft corner: *(i,j)* → *(i+1,j)* → *(i+1,j+1)*→ *(i,j+1)* → *(i,j)*.
3. Detect the core points of the fingerprint based on the result of the Poincaré index calculation, Poincaré(*i,j*) = π. Note that the detected singularities contain both concave and convex ridge core points.
4. To discriminate the detected concave ridge core point from the convex ridge core point, an algebraic summation of the absolute value of the magnitude of the local frequency orientation in the 3x3 region above the detected core points is calculated (see Figure 4(c), the cross mark is the

location of the detected core point). The point that gives the maximum calculation is detected as the reference point.

5. At a finer resolution, repeat steps 1-4 and limit the process in the local neighborhood of the detected reference point from the previous resolution.

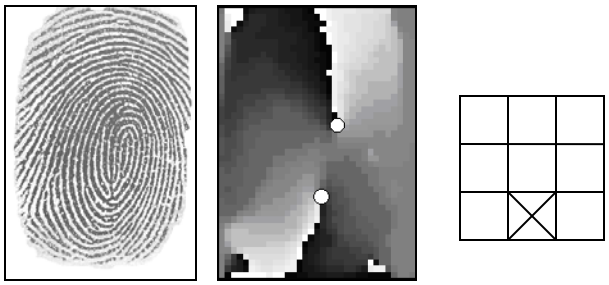

(a) (b) (c)

Figure 4: (a) A given fingerprint image. (b) The magnitude frequency orientation of (a). The circles marked in (b) are the detected core points. (c) The 3x3 region used for discriminating a concave ridge core point from a convex ridge core point.

6. TESTING RESULTS

Our reference point detection algorithm was implemented and tested on FVC 2000 Database 2 [11] and the database from [12]. We estimated the average inter-ridge distance of the fingerprints in the FVC 2000 database 2 and [12] to 10 and 7 pixels respectively. Figure 5 shows some example results from applying our algorithm on sample fingerprints. We then compared the performance of our algorithm with the algorithm proposed in [6]. We asked the third person who did not know our algorithm to manually point out the reference points of all 880 fingerprints in the FVC 2000 database 2 and 168 fingerprints in database from [12]. Arch type fingerprints in the database were removed from the test because they have no core points. The Euclidian distances between the detected reference points from both algorithms and the manually detected reference points were calculated. The comparison results are shown in table 1.

FVC 2000 DB2	Average distance from manually detected reference point (pixel)	Standard Deviation
Proposed algorithm	16.35	22.30
Algorithm from [6]	26.45	29.91
Database from [12]	Average distance from manually detected reference point (pixel)	Standard Deviation
Proposed algorithm	12.87	9.10
Algorithm from [6]	45.04	48.34

Table 1: Comparison summary.

7. CONCLUSION

For the first time, fingerprint analysis is performed in the computed AM-FM modulation domain. The experimental results showed that the proposed algorithm surpassed the method proposed in [6]. In conclusion, the proposed algorithm is efficient and feasible.

REFERENCES

[1]. J.P. Havlicek, D.S. Harding, and A.C. Bovik, "The multi-component AM-FM image representation," *IEEE Trans. Image Proc.*, vol. 5, no. 6, pp. 1094-1100, Jun. 1996.

[2]. J.P. Havlicek, D.S. Harding, and A.C. Bovik, "Multidimensional quasi-eigenfunction approximations and multicomponent AM-FM models," *IEEE Trans. Image Proc.*, vol. 9, no. 2, pp. 227-242, Feb. 2000.

[3]. J.P. Havlicek and A.C. Bovik, "Image Modulation Models," *Handbook of Image and Video Processing*, A.C. Bovik, ed., Communications, Networking, and Multimedia Series by Academic Press, San Diego, 2000, pp. 305-316.

[4]. J.P. Havlicek, A.C. Bovik, and D. Chen, "AM-FM Image Modeling and Gabor Analysis," in *Visual Information Representation, Communication, and Image Processing,* C.W. Chen and Y. Zhang, eds., Marcel Dekker, New York, 1999.

[5]. J.P. Havlicek, J.W. Havlicek, and A.C. Bovik, "The analytic image," in *Proc. IEEE Int. Conf. Image Processing*, Santa Barbara, CA, Oct. 26-29, 1997.

[6]. A.K. Jain, S. Prabhakar, L. Hong, and S. Pankanti, "Filterbank-Based Fingerprint Matching," *IEEE Trans. Image Proc.*, vol. 9, no. 5, pp. 846-859, May 2000.

[7]. R.C. Gonzales and R.E. Woods, *Digital Image Processing*, Addision-Wesley, Reading, MA, 1992.

[8]. M. Kass and A. Witkin, "Analyzing Oriented Patterns", *Computer Vision, Graphics, and Image Processing*, vol. 37, pp. 362-385, 1987.

[9]. A.R. Rao, *A Taxonomy for Texture Description and Identification*, Springer-Verlag, New York, 1990.

[10]. M. Kawagoe and A. Tojo, "Fingerprint pattern classification", *Pattern Recognition*, vol. 17, pp. 295-303.

[11]. D. Maio, D. Maltoni, R. Cappelli, J.L. Wayman, and A.K. Jain, "FVC2000: Fingerprint Verification Competition," Biolab internal report, Univ. of Bologna, Italy, Sept. 2000, available at http://bias.csr.unibo.it/fvc2000/.

[12]. Biometrics Systems Lab., University of Bologna, Cesena-Italy, http://www.csr.unibo.it/research/biolab/bio_tree.html.

Figure 5: Example results from applying the proposed algorithm on sample fingerprints from FVC 2000 Database 2.